https://dx.doi.org/10.21577/0103-5053.20200118

J. Braz. Chem. Soc., Vol. 31, No. 10, 2155-2163, 2020
Printed in Brazil - ©2020 Sociedade Brasileira de Química

Article

Theoretical Calculations on the Mechanism of Hydrogenation of Diphenylacetylene over Pd_n (n = 1-4) Clusters

Yan Chen, *,[a] *Yong Fang,*[b] *Jinglong Pan,*[c] *Hao Fu*[c] *and Wen Cao*[a]

[a]*School of Information Engineering, Southwest University of Science and Technology, 621000 Mianyang, Sichuan, China*

[b]*Key Laboratory of Green Chemistry and Technology, Ministry of Education, College of Chemistry, Sichuan University, 610064 Chengdu, Sichuan, China*

[c]*Institute of Machinery Manufacturing Technology, China Academy of Engineering Physics, 621000 Mianyang, Sichuan, China*

Diphenylacetylene (DPA) is a precursor of stilbene and benzil, and reduction of DPA or its derivatives with metallic reagents is both an old and contemporary topic of research. By means of density function theory (DFT) calculations, a detailed investigation of the mechanism of the hydrogenation of DPA over Pd clusters was carried out at the molecular level. The various species structures in the hydrogenation of DPA over Pd clusters were optimized and analyzed. The calculations indicate that the reactions over different Pd clusters share similar reaction mechanisms, and the entire reaction path could be divided into approximately two stages: stage 1: the hydrogenation of DPA to stilbene by the addition of one hydrogen molecule; and stage 2: the hydrogenation of stilbene to the final product diphenylethane (DPE) with the recovery of the catalyst. The Pd_2- and Pd_3-catalyzed systems exhibit the smallest rate-determining step (RDS) energy barrier, and these systems might be the most active and effective catalytic species among the Pd clusters. Although the Pd clusters used in the current work are simple systems, these clusters could eventually provide insights into the specific structure of the Pd catalyst, since Pd and/or clusters and/or nanoparticles could be envisioned as active catalysts in experiments.

Keywords: palladium-catalyzed, diphenylacetylene, DFT, reaction mechanisms

Introduction

The carbon-carbon triple bond of alkynes is one of the basic functional groups in chemistry, and its reaction belongs to the foundations of organic chemistry.[1-3] In recent years, the physical chemistry and theory of few organic molecules have been studied more deeply than those of acetylene. Acetylene chemistry has undergone a renaissance because acetylene not only is present in molecules on the frontiers of organic chemistry, such as pharmaceutical chemistry and biochemistry, but also serves as a building block or a general intermediate for the synthesis of large numbers of chemicals.[4-6] The development of new synthetic methodologies based on transition metal catalysis has provided impetus to alkyne chemistry.[7] The partial hydrogenation catalytic reduction of internal alkynes is an efficient method for preparing olefins and alkanes, and metal complex catalysts have been the most effective catalysts for achieving this transformation.[8,9] The methods for the hydrogenation of alkynes provide exciting strategies for the synthesis of complex organic building blocks and attract extensive attention in pharmaceuticals and other valuable chemicals. This type of hydrogenation reaction utilizes homogeneous Ni, Cr, Ru, Rh, Pd, Cu and borate organic catalysts and is known for the reduction of olefins, alkynes, nitriles and ketones. Although hydrogenation reagents are hydrogen activated by transition metal-based catalysts, Pd catalysts require the mildest of conditions and are the most widely used.[10-14]

Diphenylacetylene (DPA) is particularly representative of the alkynes, and it can act as a Lewis acid and ligand in organometallic chemistry because of its symmetry and high planarity. Additionally, DPA is a precursor of stilbene and benzil and reduction of DPA or its derivatives with metallic reagents is old and contemporary topic of research; much attention has been focused on metal complexes, such as

*e-mail: ychen@swust.edu.cn

Pd, Ir, Ag, Rh complexes, etc.,[15-20] as reductants. In the case of the hydrogenation reaction of diphenylacetylene, however, diphenylethylene is formed as a primary product, but 1,2-diphenylethane (DPE) is absent. In addition, with the development of chemistry, some different synthetic methods, such as the reduction of diphenylacetylene to 1,2-diphenylethane, have been discovered. Recent methods for the synthesis of 1,2-diphenylethane have concentrated on the direct reduction of diphenylacetylene, and most of the reported methods require metal complexes. For example, Cravotto and co-workers[21] reported that the Pd complex can act as a catalyst to generate 1,2-diphenylethane by the reduction of diphenylacetylene. Additionally, Webster and co-workers[22] reported that using the Fe^{II} complex as a catalyst, in 1 equivalent of $^nBuNH_2$ and HBpin, the triple bond was reduced, and the 1,2-diphenylethane was obtained. However, low yield and many byproducts affect the efficient utilization of catalysts in the hydrogenation of diphenylacetylene. A new hydrogenation reaction with complex metal catalysts was reported by Jackowski and co-workers.[20] When $Cl_2Pd(PPh_3)_2/Me_2Zn$ was used as the catalyst in the reduction of diphenylacetylene, 1,2-diphenylethane was the only product and was produced in 99% yield. Despite the use of a bimetallic complex in hydrogenation reactions, $Cl_2Pd(PPh_3)_2$ as precatalyst and Me_2Zn as a reducing agent, Me_2Zn interacts with the Pd^{II} precatalyst to deliver $Cl_2Pd(PPh_3)_2$, which is reduced to Pd^0.[20] Therefore, Pd^0 is an efficient catalyst in the hydrogenation of diphenylacetylene to 1,2-diphenylethane. Although the authors deduced the reaction mechanism by experiments, the details of the transformations and, more importantly, the origins of the observed selectivity still need to be understood at the molecular level, without which the mechanism of the calculations is incomplete. In challenging situations, the preferred mechanism may depend on the reaction conditions and ligands. While experiments can provide sufficient insights, the interpretation of these results is often inconclusive. In such cases, moving to computational chemistry may attain a deeper understanding of specific chemical problems.

In many cases, Pd catalysis has provided a new world of transformations and has made numerous structural parts more accessible. Although the role of Pd may be apparent, there are usually multiple pathways that need to be considered.[14,23-27] With the progress of theoretical methods in recent years, the combination of quantum chemical computations and experiments has made great progress in the development of chemistry. Particularly, the density functional theory (DFT) method[28-33] has been widely used in the study of the mechanisms, molecular interactions, and origins of selectivity in the reactions.

Here, we have employed the DFT method to investigate the mechanism of the reduction reaction at a molecular level. The aim of the present paper is focused on the following aspects: (*i*) the most feasible step of the whole reaction, including the rate-determining step (RDS); (*ii*) the effect of the states of the palladium catalysts (Pd-Pd_4) on the hydrogenation reaction (Scheme 1); and (*iii*) the configuration of the stilbenes (semihydrogenation products). This computational study contributes to the understanding of these hydrogenation reactions at the molecular level and can also provide some important suggestions for new hydrogenation reactions.

Methodology

The previous computational literatures demonstrated that the density functional Minnesota 06 (M06)[34-37] and Becke, 3-parameter, Lee-Yang-Parr (B3LYP)[38,39] methods performed well for catalytic reactions based on the transition metal system.[33,40-45] In the present investigations, the geometrical optimizations of all the intermediates (IM) and transition states (TS) were performed using the M06 and B3LYP methods, respectively. The palladium clusters were optimized before the coordination of DPA, the initial Pd–Pd distances of 1.5 and 3 Å were used in the optimization of Pd agglomerates and the coordinates of palladium atoms of the clusters were relaxed in following optimization. The electronic spin state of the considered Pd_n clusters is the singlet state. The SDD basis set[46] was used for Pd atom and the 6-311+G(d,p) basis set[47] was employed for the rest atoms. The solvation effect was considered in the geometry optimization by a self-consistent reaction field (SCRF), in which the polarizable continuum model (PCM) implicit solvent model was employed with tetrahydrofuran (THF) as a solvent.[48-50] All geometries were optimized in

Pd clusters = Pd_1, Pd_2, Pd_3 or Pd_4

Scheme 1. Pd-catalyzed hydrogenation of diphenylacetylene to 1,2-diphenylethane.

vacuum by using PCM model. This model was used for single-point energy calculations based on all of the solvent-phase optimized geometries at a larger basis set (SDD for the Pd atom and 6-311+G(d,p) for other atoms). All DFT calculations were performed with the Gaussian 09[51] series of electronic structure programs. The vibrational frequencies were assessed at the same level of theory as that for the geometrical optimizations, to verify the stationary points as local minima (no imaginary frequencies) or transition states (unique imaginary frequency). Necessarily, using the intrinsic reaction coordinate (IRC) method,[52] the key transition states were confirmed to be the connection between the corresponding reactant and product. The total cartesian coordinates for all minima point and transition states in the gas-phase by B3LYP and M06 are provided in the Supplementary Information (SI) section.

Results and Discussion

Reaction mechanism

The DFT calculations predicted that the reactions over different Pd clusters share a reaction mechanism similar to that in Scheme 1, and the entire reaction path could be divided into approximately two successive stages: stage 1: the hydrogenation of DPA to stilbene by the addition of one hydrogen molecule; and stage 2: the hydrogenation of stilbene to the final product DPE with the recovery of the catalyst.

Additionally, M06 and B3LYP gave the comparable values with few discrepancies in the optimized geometries, which implies that the present calculation is reasonable for the titled reaction system. To give a concise expression, the following discussion will be based on the Pd_3-catalyst system at the B3LYP(PCM)/6-311+G(d,p), SDD level unless otherwise specified. The detailed information about the optimized structures and energy profile of the hydrogenation of DPA over the Pd, Pd_2 and Pd_4 cluster systems is provided in the SI section.

Stage 1: hydrogenation of DPA to stilbene

The energy profile and the optimized IMs and TSs at the B3LYP/6-311+G(d,p), SDD, are shown in Figure 1.

As shown in Figure 1, the reaction is triggered by the coordination of the alkyne moiety with the Pd atoms with the formation of the Pd_3-DPA complex, and the palladium clusters were optimized before its approximation to DPA. In this complex, the Pd–C distances are calculated to be 1.99-2.14 Å, and the negative Laplacian of electronic densities $\nabla^2\rho$ at (3, –1) bonding critical points by atoms in molecule (AIM) analysis[53] in Figure 2 indicates the covalent interaction between Pd_3 and DPA, demonstrating that there is a strong interaction between the substrate and the Pd_3 cluster. This result could be enhanced by the lower relative free energy of 54.7 kcal mol^{-1} with respect to the separated substance and bare Pd_3 cluster.

Next, an external H_2 molecule gets close to one Pd-end of the Pd_3-DPA complex and leads to the yield of Pd_3-IM^1

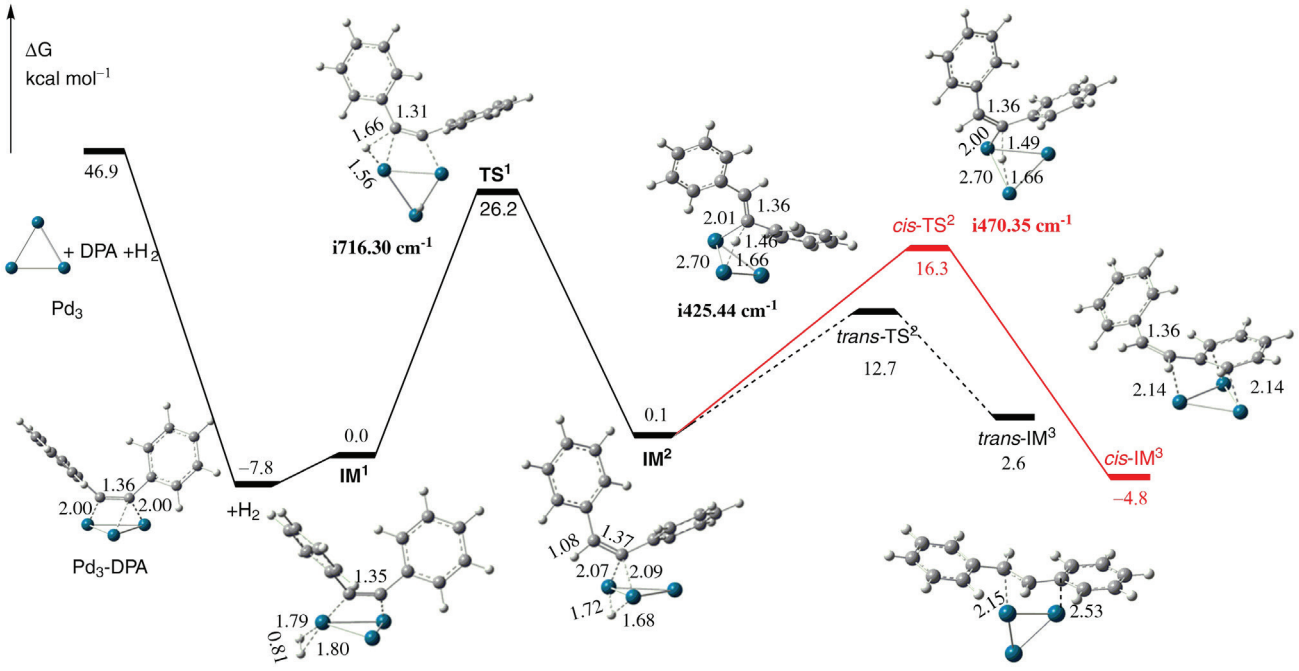

Figure 1. 3D models of various species and the energy profile in reaction stage 1 of Pd_3-catalyzed hydrogenation of diphenylacetylene (DPA) system obtained at the M06/6-311+G(d,p), SDD level. Bond lengths are in Å, relative energies are in kcal mol^{-1} and imaginary frequencies are in cm^{-1}.

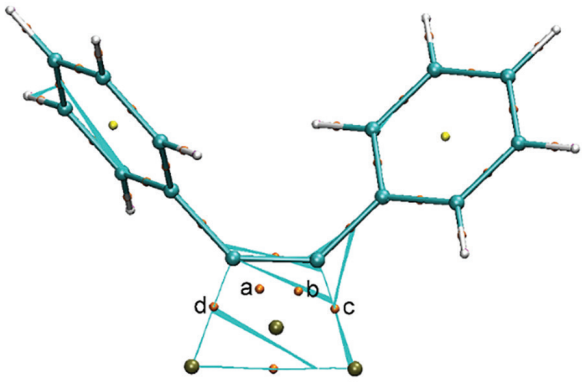

Figure 2. Laplacian ($\nabla^2\rho$) and electronic density (ρ) of selected bond critical points (BCP) for Pd_3-DPA complex were obtained by atoms in molecule (AIM) analysis.

intermediate. In this IM, the H–H bond is slightly enlarged to 0.81 Å, and the Pd–H distances are predicted to be ca. 1.79 Å. The formation of the Pd_3-IM^1 is calculated to be energy-favored by −7.8 kcal mol^{-1} from Pd_3-DPA + H_2, indicating that the generation of Pd_3-IM^1 from reactants is non-spontaneous.

Then, the cleavage of the H–H bond and the insertion of one hydrogen atom into the DPA takes place through the three-membered ring transition state (TS^1), leading to the formation of Pd_3-IM^2. In this species, the three-membered ring is characterized by an elongated C–H bond of 1.66 Å, Pd–C bond of 2.08 Å and Pd–H bond of 1.56 Å. For Pd_3-IM^2, the C–H distance is calculated to be 1.08 Å, indicating that the migration of hydrogen atom is complete, and the corresponding C–H bond has been formed. In addition, the rest of the alkyne coordinates with the two Pd ends of the Pd_3 cluster with the Pd–C distances of 2.09 Å. The calculations show that the above step has a moderate energy barrier of 26.2 kcal mol^{-1}.

From the Pd_3-IM^2, the next hydrogen atom transfers to another side of the alkyne moiety of the DPA via transition state TS^2, which leads to the formation of Pd_3-IM^3. As shown in Figure 1, *cis*-TS^2 and *trans*-TS^2 are located on the energy profile: the former leads to the stilbene moiety in the *E*-configuration in the *cis*-IM^3 intermediate, and the latter leads to the *Z*-configuration in the *trans*-IM^3 intermediate. Each TS^2 features the four-membered ring transition state with the Pd–Pd bond of ca. 2.70 Å, Pd–C bond of ca. 2.00 Å, C–H bond of ca. 1.50 Å and H–Pd bond of 1.70 Å.

As a result, *cis*- and *trans*-IM^3 are identified at the end of stage 1 of the reaction mechanism. For each IM^3, the C–H distance is calculated to be ca. 1.09 Å, indicating that the migration of the hydrogen atom is finished, and the corresponding C–H bond has been formed. In addition, the alkene that is generated coordinates with the Pd_3 cluster with the Pd–C distances in the range of 2.14-2.15 Å, demonstrating the interaction between the carbon of the phenyl ring and the Pd_3 cluster. As a result, the stilbene adsorbed on the Pd_3 cluster is generated at the end of this reaction state after TS^2, and the energy barrier of the step via TS^2 is calculated to be 16.3 kcal mol^{-1} for the *cis*-path and 12.7 kcal mol^{-1} for the *trans*-path.

Here, it should be emphasized that the configuration of the stilbene intermediate is closely dependent on the step via the TS^2, and therefore the TS^2 appears to be the stereo-controlling transition state in the reaction stage 1. The B3LYP calculation predicts the energy barrier via the *trans*-TS^2 is energy-favored by 3.6 kcal mol^{-1} over its competing transition state of *cis*-TS^2. The *trans*-TS^2 links to the formation of stilbene in the *Z*-configuration and the *cis*-TS^2 to the formation of stilbene in the *E*-configuration, according to the absolute rate theory and the formula as follows:

$$trans : cis = k_{trans} : k_{cis} = \exp\left(-\frac{\Delta G^{\neq}_{trans}}{RT}\right) : \exp\left(-\frac{\Delta G^{\neq}_{cis}}{RT}\right) \quad (1)$$

where k is the rate constant, T is the absolute temperature, R is the gas constant, and $\Delta G^{\neq}$ is the activation Gibbs free energy.

The stereo-selectivity of stilbene is predicted to be *Z* / *E* > 1:99 at 298.15 K indicating that the generation of *Z*-stilbene might be advantageous in thermodynamics. However, considered the error generated from the DFT calculations, this reason may be not accurate enough to account for the selectivity of *cis*- and *trans*-IMs in the experiment.

Stage 2: hydrogenation of stilbene to DPE

In stage 2, the reaction must undergo the hydrogenation from stilbene to DPE over Pd-catalyst with the addition of another H_2 molecule after the reaction stage 1 has been completed. The results are shown in Figure 3.

In this stage, an external H_2 molecule coordinates to one Pd-end of two Pd_3-IM^3 complexes and leads to the yield of *cis*- or *trans*-IM^4 intermediate. In each IM^4, the H–H bond is slightly enlarged to ca. 0.85-0.86 Å, and the Pd–H distances are calculated to be ca. 1.70 Å. The formation of the *cis*-IM^4 is predicted to be energy-favored by 9.7 kcal mol^{-1} from the separated *cis*-IM^3 and H_2, and the formation of the *trans*-IM^4 is calculated to be favored by 12.0 kcal mol^{-1} from the separated *trans*-IM^3 and H_2 in relative energy, indicating that the generation of IM^4 is spontaneous.

Next, the breakage of the H–H bond and the insertion of one hydrogen atom into the stilbene moiety occur through

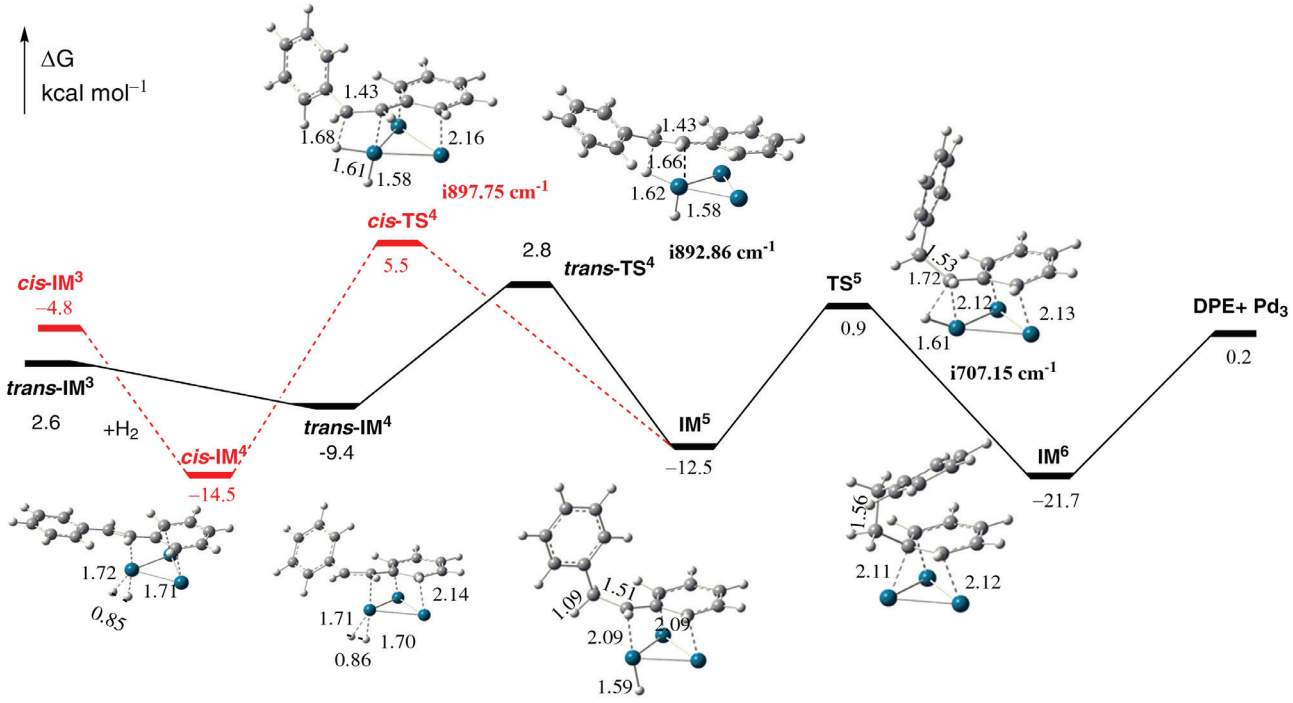

Figure 3. 3D models of various species and the energy profile in reaction stage 2 of Pd_3-catalyzed hydrogenation of diphenylacetylene (DPA) system obtained at the M06/6-311+G(d,p), SDD level. Bond lengths are in Å, relative energies are in kcal mol^{-1} and imaginary frequencies are in cm^{-1}.

the four-membered ring transition state (*cis*- or *trans*-TS^4) with the generation of the IM^5. The four-membered ring is characterized by an elongated C–H bond of 1.66-1.68 Å, Pd–H bond of 1.61-1.62 Å, Pd–C bond of ca. 2.10 Å, and C–C bond of 1.43 Å. For IM^5, the calculations determine the optimized C–H distance to be 1.09 Å, which implies that the transfer of the hydrogen atom is completed with the formation of the corresponding sp^3 carbon. In addition, the rest of the alkene part coordinates the two Pd atom Pd_3 cluster with the Pd–C distances of ca. 2.09 Å. The calculations predict that the above step has a moderate energy barrier of 12.5 kcal mol^{-1} in relative energy.

Then, from the IM^5, the reaction goes through the four-membered ring transition state (TS^5), leading to the formation of IM^6. The three-membered ring is composed of a Pd–C bond of 2.13 Å, a C–H bond of 1.73 Å and a H–Pd bond of 1.61 Å. For IM^6, the C–H distance is calculated to be 1.09 Å, indicating that the migration of the hydrogen atom is completed, and the corresponding C–H bond is formed. In addition, the rest of the alkyne coordinates with the three Pd atom Pd_3 cluster with the Pd–C distances of ca. 2.12 Å. The calculations indicate that the above step has a moderate energy barrier of 13.4 kcal mol^{-1}.

Finally, the release of DPE from IM^6 takes place with the recovery of the Pd_3-cluster. This step is predicted to be endothermic by ca. 21.9 kcal mol^{-1} without any barrier. As shown in Figures 1 and 3, the entire reaction is clearly favored by 54.7 kcal mol^{-1} in Gibbs free energy, and the largest barrier of 26.2 kcal mol^{-1} corresponds to the step from the $IM^1 \rightarrow TS^1$, indicating that the first hydrogenation step should be the rate determining step (RDS).

Comparison of Pd-Pd_4 catalyzed reactions

The reaction mechanisms over the Pd-Pd_4 cluster are similar, but the properties of the energy profiles vary: for the Pd-Pd_3 systems, both the M06 and B3LYP calculations predict that the step of $IM^1 \rightarrow TS^1$ is the RDS with the barrier of ca. 22-29 kcal mol^{-1} (see SI section), while the RDS of the Pd_4 system turns to the final hydrogen migration step in $IM^5 \rightarrow TS^5$ with the giant barrier larger than 33 kcal mol^{-1}. It is found that B3LYP energies could be considerably underestimated, and this is in accordance with the literature.[54,55] The 3D models of various species and the energy profile are shown in Figures 4 and 5.

Analysis of turnover frequency (TOF) in the catalytic cycle

In addition, based on the transition state theory and energetic span model,[56] we evaluated the theoretical turnover frequency (TOF) of the catalytic cycle via the intermolecular and H-transfer mechanism catalyzed by the Pd_n (n = 1-4) catalyst. In equations 2 and 3,[57-60] the δE (energy span) is the energy difference between the summit and the through of the catalytic cycle. GTDTS and GTDI are defined as the Gibbs free energy of the

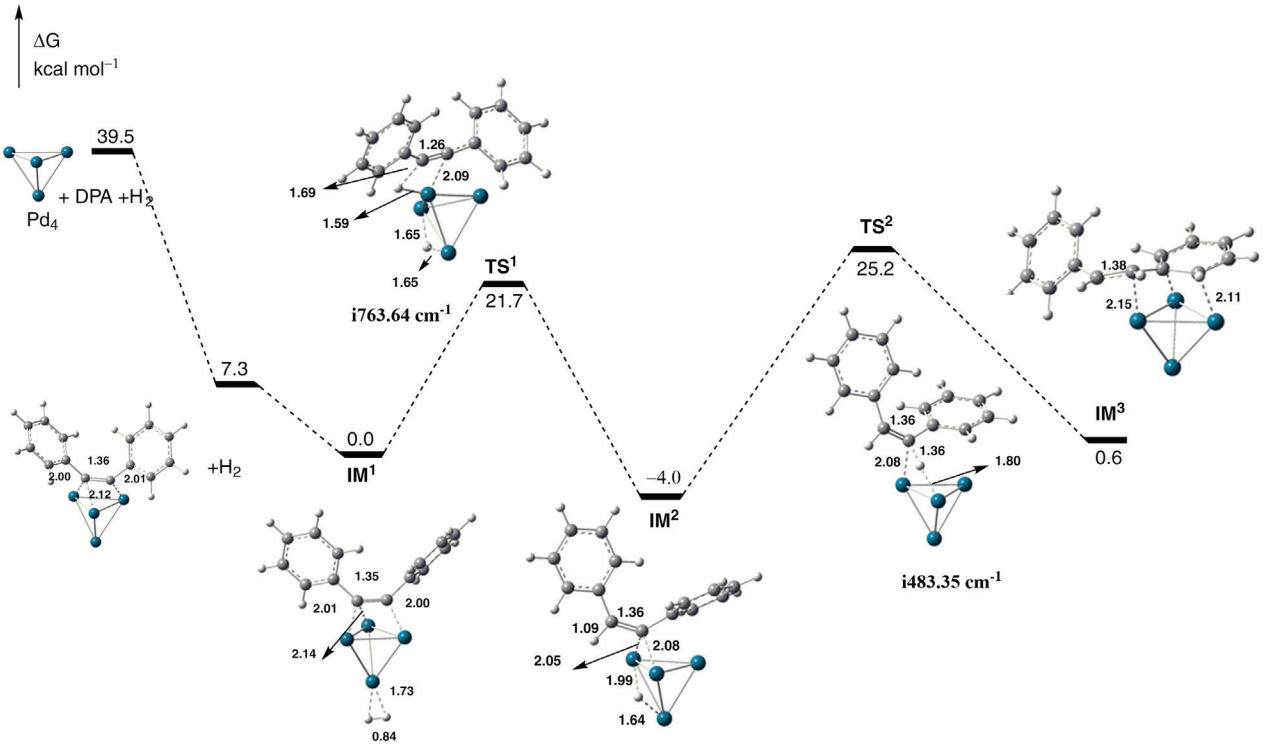

Figure 4. 3D models of various species and the energy profile in reaction stage 1 of Pd_4-catalyzed hydrogenation of diphenylacetylene (DPA) system obtained at the M06/6-311+G(d,p), SDD level. Bond lengths are in Å, relative energies are in kcal mol^{-1} and imaginary frequencies are in cm^{-1}.

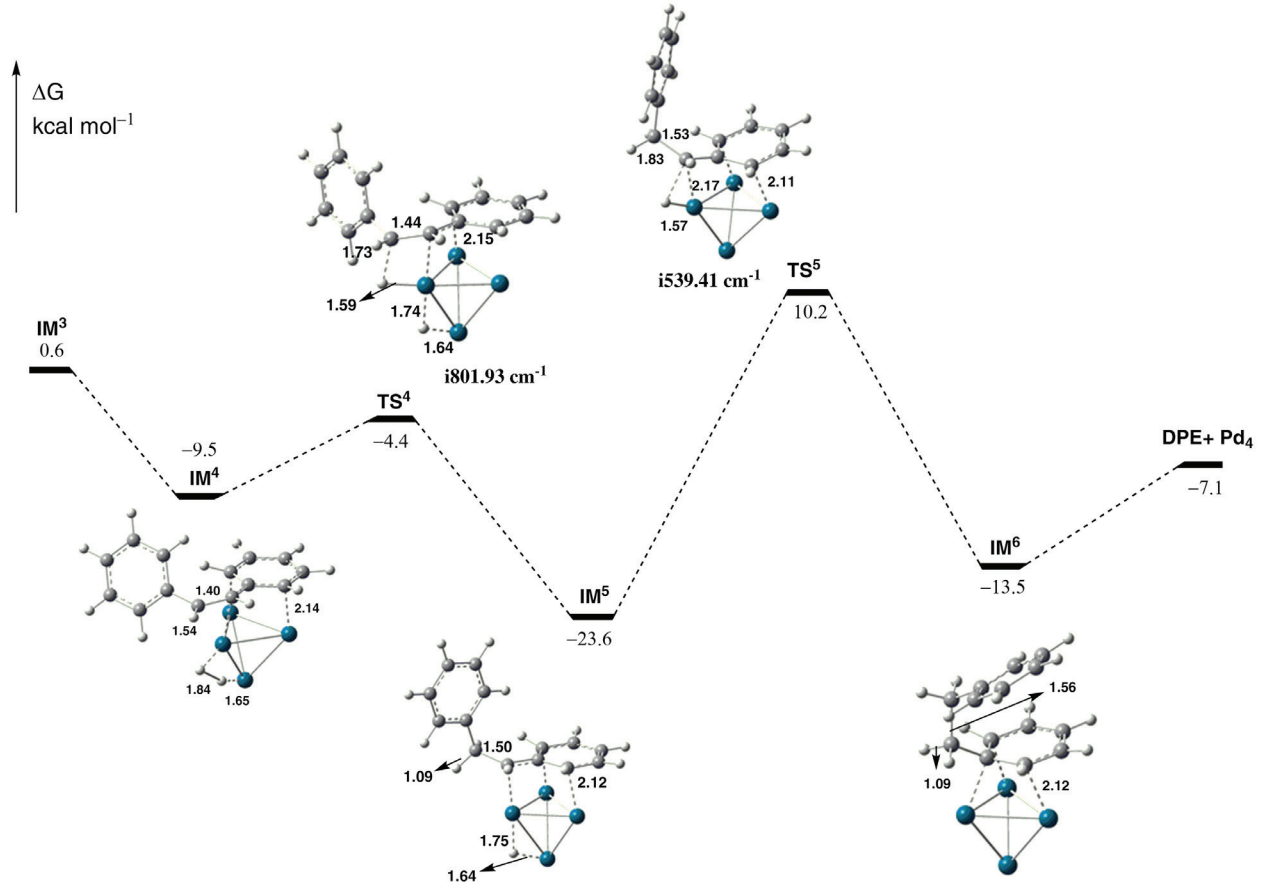

Figure 5. 3D models of various species and the energy profile in reaction stage 2 of Pd_4-catalyzed hydrogenation of diphenylacetylene (DPA) system obtained at the M06/6-311+G(d,p), SDD level. Bond lengths are in Å, relative energies are in kcal mol^{-1} and imaginary frequencies are in cm^{-1}.

TOF-determining transition state (TDTS) and the TOF-determining intermediate (TDI), and ΔG_r is the global free energy of the whole cycle.[56,61]

$$TOF \approx \frac{K_B T}{h} e^{-\delta E/RT} \quad (2)$$

where K_B is Boltzmann's constant, h is Planck's constant, T is the absolute temperature, R is the gas constant, and

$$\delta E = E(TDTS) - E(TDI), \text{ if TDTS appears after TDI} \quad (3)$$

$$\delta E = E(TDTS) - E(TDI) + \Delta G_r, \text{ if TDTS appears before TDI} \quad (4)$$

As shown in Table 1, the intermediate $IM^1 + H_2$ and IM^5 is predicted to be TDI, and the H-transfer transition states TS^1 and TS^5 are TDTS for the whole cycle of the hydrogenation reaction. As expected, the TOFs of the catalytic cycles involving Pd_n (n = 1-4) catalyzed H-transfer pathways are significantly higher than that of the intramolecular H-transfer pathways. Moreover, Pd_3 exhibits better catalytic performance when the catalytic reaction occurs along the Pd_3 reaction pathway, with TOF being 0.25 s^{-1}.

Table 1. Turnover frequency (TOF) of the catalytic cycle for hydrogenation reaction catalyzed by Pd_n (n = 1-4) along four paths

Catalyst	TDI	TDTS	TOF / s^{-1}
Pd	$IM^1 + H_2$	TS^1	3.45×10^{-5}
Pd_2	$IM^1 + H_2$	TS^1	2.14×10^{-1}
Pd_3	$IM^1 + H_2$	TS^1	2.46×10^{-1}
Pd_4	IM^5	TS^5	8.90×10^{-8}

TDI: TOF-determining intermediate (IM); TDTS: TOF-determining transition states.

Conclusions

The mechanism of the hydrogenation reaction of diphenylacetylene catalyzed by Pd-Pd_4 species was investigated by using DFT method. The entire reaction mechanism in the present investigation is predicted to be composed of two processes: stage 1: the hydrogenation of DPA to stilbene with the addition of one hydrogen molecule via TS^1 and TS^2; and stage 2: the hydrogenation of stilbene via TS^3 and TS^4 to the final product DPE with the recovery of the catalyst.

The calculation on the diphenylacetylene system indicates that the hydrogenation could take place in existence of four catalysis of Pd, Pd_2, Pd_3 and Pd_4. For the Pd-Pd_3 systems, both the M06 and B3LYP calculations predict that the step of $IM^1 \rightarrow TS^1$ is the RDS with the barrier of the largest Gibbs energy, and the RDS of the Pd_4 system turns to the step of the final hydrogen-migration step in $IM^5 \rightarrow TS^5$ with the giant barrier larger than 33.1 kcal mol^{-1}. The calculation reproduces the major product *E*-stilbene intermediate, and exhibits the smallest RDS energy barrier for the Pd_2- and Pd_3-catalyzed system. Therefore, Pd_2- and Pd_3-catalysts might be the most active and effective catalysis species among the four clusters. This computational study is expected to provide a full understanding of this hydrogenation reaction at the molecular level and can also provide some important suggestions for the rational design and synthesis of the new Pd-catalytic hydrogenation reactions.

Supplementary Information

The total Cartesian coordinates for all minima point and transition states in the gas phase by B3LYP and M06 are available free of charge at http://jbcs.sbq.org.br as PDF file.

Acknowledgments

This research was funded by Academy-School Cooperation Project S18H321-Q.

Author Contributions

Yan Chen was responsible for the conceptualization, data curation, validation, formal analysis, funding acquisition and writing orignal draft; Yong Fang for the data curation, software and writing original draft; Jinglong Pan for the software and writing review and editing; Hao Fu for the writing review and editing; Wen Cao for the formal analysis, funding acquisition and writing review and editing.

References

1. Jun, C. H.; *Chem. Soc. Rev.* **2004**, *33*, 610.
2. Tobisu, M.; Chatani, N.; *Chem. Soc. Rev.* **2008**, *37*, 300.
3. Wang, A.; Jiang, H.; *J. Am. Chem. Soc.* **2008**, *130*, 5030.
4. Chinchilla, R.; Najera, C.; *Chem. Rev.* **2014**, *114*, 1783.
5. Stang, P. J.; Diederich, F.; *Modern Acetylene Chemistry*; VCH: Weinheim, 1995.
6. Diederich, F.; Stang, P. J.; Tykwinski, R. R.; *Acetylene Chemistry*; Wiley-VCH: Weinheim, 2005.
7. Schmidt, E. Y.; Tatarinova, I. V.; Semenova, N. V.; Protsuk, N. I.; Ushakov, I. A.; Trofimov, B. A.; *J. Org. Chem.* **2018**, *83*, 10272.

8. Borodziński, A.; Bond, G. C.; *Catal. Rev.* **2008**, *50*, 379.
9. Molnár, Á.; Sárkány, A.; Varga, M.; *J. Mol. Catal. A: Chem.* **2001**, *173*, 185.
10. Barrios-Francisco, R.; García, J. J.; *Appl. Catal., A* **2010**, *385*, 108.
11. Espinal-Viguri, M.; Neale, S. E.; Coles, N. T.; Macgregor, S. A.; Webster, R. L.; *J. Am. Chem. Soc.* **2019**, *141*, 572.
12. Shao, Z.; Fu, S.; Wei, M.; Zhou, S.; Liu, Q.; *Angew. Chem., Int. Ed.* **2016**, *55*, 14653.
13. Zhou, Q.; Zhang, L.; Meng, W.; Feng, X.; Yang, J.; Du, H.; *Org. Lett.* **2016**, *18*, 5189.
14. Sperger, T.; Sanhueza, I. A.; Kalvet, I.; Schoenebeck, F.; *Chem. Rev.* **2015**, *115*, 9532.
15. Kojima, Y.; Matsuoka, T.; Takahashi, H.; *J. Mater. Sci. Lett.* **1996**, *15*, 1543.
16. Li, S. H.; Li, L. C.; Xu, C. H.; *Chin. Chem. Lett.* **2012**, *23*, 69.
17. Manna, S.; Antonchick, A. P.; *ChemSusChem* **2019**, *12*, 3094.
18. Domínguez-Domínguez, S.; Berenguer-Murcia, Á.; Linares-Solano, Á.; Cazorla-Amorós, D.; *J. Catal.* **2008**, *257*, 87.
19. Nishio, R.; Sugiura, M.; Kobayashi, S.; *Org. Biomol. Chem.* **2006**, *4*, 992.
20. Maazaoui, R.; Abderrahim, R.; Chemla, F.; Ferreira, F.; Perez-Luna, A.; Jackowski, O.; *Org. Lett.* **2018**, *20*, 7544.
21. Wu, Z.; Cherkasov, N.; Cravotto, G.; Borretto, E.; Ibhadon, A. O.; Medlock, J.; Bonrath, W.; *ChemCatChem* **2015**, *7*, 952.
22. King, A. K.; Buchard, A.; Mahon M. F.; Webster, R. L.; *Chem. - Eur. J.* **2015**, *21*, 15960.
23. Sameera, W. M. C.; Maseras, F.; *Wiley Interdiscip. Rev.: Comput. Mol. Sci.* **2012**, *2*, 375.
24. Bonney, K. J.; Schoenebeck, F.; *Chem. Soc. Rev.* **2014**, *43*, 6609.
25. Holder, J. C.; Zou, L.; Marziale, A. N.; Liu, P.; Lan, Y.; Gatti, M.; Kikushima, K.; Houk, K. N.; Stoltz, B. M.; *J. Am. Chem. Soc*. **2013**, *135*, 14996.
26. Lan, Y.; Houk, K. N.; *J. Org. Chem.* **2011**, *76*, 4905.
27. Musaev, D. G.; Figg, T. M.; Kaledin, A. L.; *Chem. Soc. Rev.* **2014**, *43*, 5009.
28. Kohn, W.; Sham, L. J.; *Phys. Rev.* **1965**, *140*, 1133.
29. Dreizler, R. M.; Gross, E. K. U.; *Density Function Theory*; Springer: Berlin, 1990.
30. Steinmetz, M.; Grimme, S.; *ChemistryOpen* **2013**, *2*, 115.
31. Koch, W.; Holthausen, M. C.; Kaupp, M.; *Angew. Chem.* **2001**, *113*, 989.
32. Dreizler, R. M.; Gross, E. K. U.; *Density Functional Approach to Time-Dependent and to Relativistic Systems*; Springer: Boston, 1985.
33. Lipshutz, B. H.; Chrisman, W.; Noson, K.; Papa, P.; Sclafani, J. A.; Vivian, R. W.; Keith, J. M.; *Tetrahedron* **2000**, *56*, 2779.
34. Zhao, Y.; Truhlar, D.; *Theor. Chem. Acc.* **2008**, *120*, 215.
35. Zhao, Y.; Truhlar, D.; *Acc. Chem. Res.* **2008**, *41*, 157.
36. Bryantsev, V. S.; Diallo, M. S.; van Duin, A. C. T.; Goddard III, W. A.; *J. Chem. Theory Comput.* **2009**, *5*, 1016.
37. Jacquemin, D.; Perpète, E. A.; Ciofini, I.; Adamo, C.; Valero, R.; Zhao, Y.; Truhlar, D. G.; *J. Chem. Theory Comput.* **2010**, *6*, 2071.
38. Becke, A. D.; *J. Chem. Phys.* **1993**, *98*, 5648.
39. Lee, C. T.; Yang, W. T.; Parr, R. G.; *Phys. Rev. B: Condens. Matter Mater. Phys.* **1988**, *37*, 785.
40. Shi, S. L.; Xu, L. W.; Oisaki, K.; Kanai, M.; Shibasaki, M.; *J. Am. Chem. Soc.* **2010**, *132*, 6638.
41. Liu, H. Y.; Zhang, W.; He, L.; Luo, M. L.; Qin, S.; *RSC Adv.* **2014**, *4*, 5726.
42. Zhang, W.; Li, W. Y.; Qin, S.; *Org. Biomol. Chem.* **2012**, *10*, 597.
43. Hong, S.; Huber, S. M.; Gagliardi, L.; Cramer, C. C.; Tolman, W. B.; *J. Am. Chem. Soc.* **2007**, *129*, 14190.
44. Bar-Nahum, I.; Gupta, A. K.; Huber, S. M.; Ertem, M. Z.; Cramer, C. J.; Tolman, W. B.; *J. Am. Chem. Soc.* **2009**, *131*, 2812.
45. Cramer, C. J.; Gour, J. R.; Kinal, A.; Wloch, M.; Piecuch, P.; Shahi, A. R. M.; Gagliardi, L.; *J. Chem. Phys. A* **2008**, *112*, 3754.
46. Igel-Mann, G.; Stoll, H.; Preuss, H.; *Mol. Phys.* **1988**, *65*, 1321.
47. Frisch, M. J.; Pople, J. A.; Binkley, J. S.; *J. Chem. Phys.* **1984**, *80*, 3265.
48. Tomasi, J.; Mennucci, B.; Cancès, E.; *J. Mol. Struct.: THEOCHEM* **1999**, *464*, 211.
49. Barone, V.; Cossi, M.; *J. Phys. Chem. A* **1998**, *102*, 1995.
50. Cossi, M.; Rega, N.; Scalmani, G.; Barone, V.; *J. Comput. Chem.* **2003**, *24*, 669.
51. Frisch, M. J.; Trucks, G. W.; Schlegel, H. B.; Scuseria, G. E.; Robb, M. A.; Cheeseman, J. R.; Scalmani, G.; Barone, V.; Mennucci, B.; Petersson, G. A.; Nakatsuji, H.; Caricato, M.; Li, X.; Hratchian, H. P.; Izmaylov, A. F.; Bloino, J.; Zheng, G.; Sonnenberg, J. L.; Hada, M.; Ehara, M.; Toyota, K.; Fukuda, R.; Hasegawa, J.; Ishida, M.; Nakajima, T.; Honda, Y.; Kitao, O.; Nakai, H.; Vreven, T.; Montgomery Jr., J. A.; Peralta, J. E.; Ogliaro, F.; Bearpark, M.; Heyd, J. J.; Brothers, E.; Kudin, K. N.; Staroverov, V. N.; Keith, T.; Kobayashi, R.; Normand, J.; Raghavachari, K.; Rendell, A.; Burant, J. C.; Iyengar, S. S.; Tomasi, J.; Cossi, M.; Rega, N.; Millam, J. M.; Klene, M.; Knox, J. E.; Cross, J. B.; Bakken, V.; Adamo, C.; Jaramillo, J.; Gomperts, R.; Stratmann, R. E.; Yazyev, O.; Austin, A. J.; Cammi, R.; Pomelli, C.; Ochterski, J. W.; Martin, R. L.; Morokuma, K.; Zakrzewski, V. G.; Voth, G. A.; Salvador, P.; Dannenberg, J. J.; Dapprich, S.; Daniels, A. D.; Farkas, O.; Foresman, J. B.; Ortiz, J. V.; Cioslowski, J.; Fox, D. J.; *Gaussian 09, Revision D.01*; Gaussian, Inc., Wallingford, CT, USA, 2013.
52. Gonzalez, C.; Schlegel, H. B.; *J. Chem. Phys.* **1989**, *90*, 2154.
53. Matta, Ch. F.; Boyd, R. J.; *The Quantum Theory of Atoms in Molecules: from Solid State to DNA and Drug Design*; Wiley-VCH GmbH & Co. KGaA: Weinheim, 2007.

54. de Souza, L. A.; Nogueira, C. A. S.; Lopes, J. F.; dos Santos, H. F.; de Almeida, W. B.; *J. Phys. Chem. C* **2015**, *119*, 8394.
55. de Souza, L. A.; da Silva, A. M.; dos Santos, H. F.; de Almeida, W. B.; *RSC Adv.* **2017**, *7*, 13212.
56. Amatore, C.; Jutand, A.; *J. Organomet. Chem.* **1999**, *576*, 254.
57. Kozuch, S.; Shaik, S.; *Acc. Chem. Res.* **2011**, *44*, 101.
58. Kozuch, S.; Shaik, S.; *J. Am. Chem. Soc.* **2006**, *128*, 3355.
59. Kozuch, S.; Shaik, S.; *J. Phys. Chem. A* **2008**, *112*, 6032.
60. Uhe, A.; Kozuch, S.; Shaik, S.; *J. Comput. Chem.* **2011**, *32*, 978.
61. Qi, T.; Yang, H.-Q.; Whitfield, D. M.; Yu, K.; Hu, C.-W.; *J. Phys. Chem. A* **2016**, *120*, 918.

Submitted: December 23, 2019
Published online: June 18, 2020